Fabry-Perot tuning of the band-gap polarity in plasmonic crystals

Jin E. Kihm,[1] Y. C. Yoon,[1] D. J. Park,[1] Y. H. Ahn,[1] C. Ropers,[2] C. Lienau,[2,3] J. Kim,[4] Q. H. Park,[5] and D. S. Kim[1,*]
[1]*School of Physics and Astronomy, Seoul National University, Seoul 151-742, Korea*
[2]*Max-Born-Institut für Nichtlineare Optik und Kurzzeitspektroskopie, D-12489 Berlin, Germany*
[3]*Institut für Physik, Carl von Ossietzky Universität, D-26111 Oldenburg, Germany*
[4]*Korea Research Institute of Standards and Science, Yusung, Taejon 305-600, Korea*
[5]*Department of Physics, Korea University, Seoul 136-701, Korea*
(Received 30 June 2006; revised manuscript received 21 November 2006; published 16 January 2007)

We report experimental observation of Fabry-Perot resonances and Fabry-Perot-induced band-structure flipping in quasi-one-dimensional plasmonic crystals. Angle-resolved transmission spectra of nanoslit arrays in metal films demonstrate band-gap formation resulting from surface plasmon polariton couplings mediated via nanometer-sized waveguide channels. Tuning the waveguide dielectric function and thickness allows for a pronounced resonant enhancement of the coupling strength and band-gap energy and may even induce changes in sign of the coupling—i.e., an effective band-gap flipping. Our results indicate an interesting route towards band-gap engineering in plasmonic crystals.

DOI: 10.1103/PhysRevB.75.035414 PACS number(s): 42.70.Qs, 07.79.Fc, 42.25.−p, 73.20.Mf

The formation of electronic and photonic band gaps—i.e., energy regions with a vanishing density of states in crystalline structures—is among the most fundamental phenomena in solid-state physics, and band-gap engineering is the key to novel nanoscale functions. In semiconductor nanostructures, e.g., such engineering leads to a plethora of new physical phenomena ranging from the quantum Hall effect[1] to quantum dot lasing.[2] In photonic systems, it is essential for guiding and storing light,[3] controlling spontaneous emission,[4] and various other (quantum-)electrodynamic effects.

Recently, a new class of band-gap materials, plasmonic crystals, has been introduced[5] and sparked considerable interest. Model structures for such crystals—namely, periodic arrays of nanoholes and nanoslits in thin metal films—show surprising optical properties such as extraordinarily enhanced transmission,[5] entanglement preservation,[6] surface-plasmon-polariton- (SPP-) induced subwavelength light localization and field enhancement,[7,8] negative refractive index,[9] and possibly magnetic activity.[10] A variety of new applications have been proposed, including biosensing, surface energy transfer,[11] nanolensing,[7] and even SPP lasing.[12] Consequently, such crystals have been the subject of numerous investigations. While band-gap formation in thin metal films or periodically corrugated reflection gratings has been studied in some detail,[13] band gaps in periodic nanoslit and/or nanohole arrays are not yet well understood. Initial studies gave partly controversial results,[5,14,15] mainly because the microscopic origin of the asymmetric line shapes in the optical spectra was not resolved. Recently, much progress has been achieved in analyzing SPP excitations and their radiative damping,[14,16–18] and this has paved the way for unraveling the physical mechanisms underlying band-gap formation.

In this paper, we report experimental observation of the Fabry-Perot control of quasi-one-dimensional plasmonic band gaps. Angle-resolved linear transmission spectra of periodic nanoslit arrays in metal films show that a propagating nanocavity mode gives rise to a pronounced resonant enhancement of the plasmon-plasmon coupling and band-gap energy. We demonstrate that this cavity mode may even lead to a change in sign of the coupling—i.e., an effective *flipping* of the band gap. Our results point out a route towards band-gap engineering in plasmonic crystals.

We investigate periodic arrays of $a=100$ nm wide nanoslits in gold films of thickness $h=75$ nm deposited on a 330-μm-thick sapphire substrate. The slit array is fabricated by dry etching after *e*-beam patterning. The array period of $d=537\pm2$ nm is determined from calibrated scanning electron microscope (SEM) images and confirmed by a diffraction experiment [Fig. 1(a)]. Angle-dependent linear transmission spectra are recorded with a detection range of 400–1170 nm. The incident light was linearly (TM) polarized perpendicular to the slits. The spectra were taken with the sample being embedded in different dielectric materials with dielectric constant ϵ_d between 1 (air) and 2.69 (index matching oil).

Figure 1(c) shows angle-dependent transmission spectra of the nanoslit sample embedded in air. The spectrum reveals the typical transmission resonances due to the excitation of SPP's at either the substrate, sapphire/metal (SM), or top, dielectric/metal (DM) interfaces of the metal film. We note that all features of the transmission spectra, including resonance energies, linewidth, and shapes, and band gaps are reproducible on different spatial region of the sample.[19]

Depending on the momentum $\Delta k=pG=p2\pi/d$ (p: integer) transferred to the incident photons, these resonances are denoted as SM[p] and DM(p), respectively.[15] To first order, the SPP resonances λ_{SP}^0 are given by the SPP dispersion relation of the planar metal/dielectric interface:

$$\lambda_{SP}^0[p]=\frac{d}{p}\left(\sqrt{\frac{\epsilon_d\epsilon_m}{\epsilon_d+\epsilon_m}}\pm\sin\theta\right), \tag{1}$$

where ϵ_m and ϵ_d are the dielectric constant of the metal and dielectric, respectively, and θ the angle of incidence.

As in previous studies of two-dimensional (2D) hole arrays, the actual transmission peak wavelengths $\lambda_{SP}[p]$ for the SM[±1] band [Fig. 1(d)] appear slightly redshifted from $\lambda_{SP}^0[p]$.[5,15,16,20,21] This shift and the distinctly asymmetric line

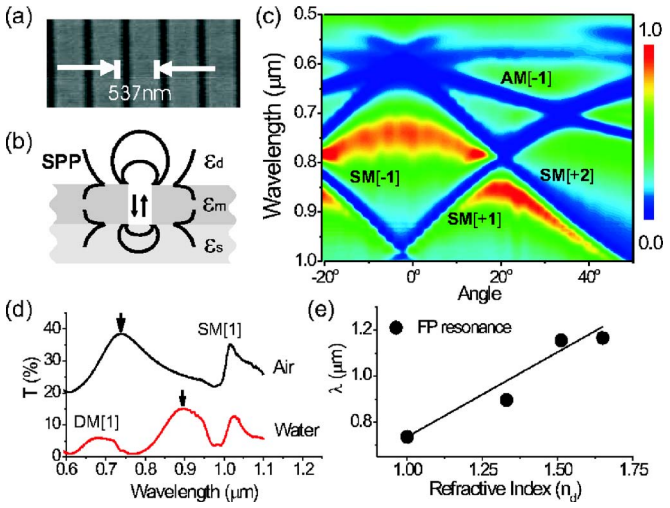

FIG. 1. (Color online) (a) SEM image of the slit sample with $d=537$ nm. (b) Sketch of the microscopic origin of Fabry-Perot (FP) resonances in transmission. (c) Angle-dependent linear transmission spectra in air. (d) Transmission spectrum at $\theta=0°$ for air (black line) and water [red (dark gray) line] as dielectric. The arrows indicate the FP resonances. (e) Experimental values of the FP resonance wavelength versus n_d and linear extrapolation.

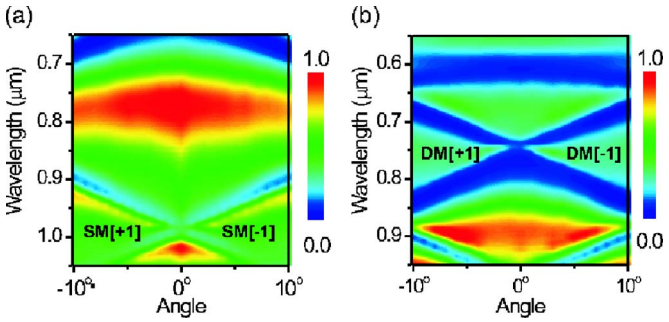

FIG. 2. (Color online) (a) Angle-dependent transmission spectra in air [Fig. 1(c)], in a narrow range around the SM[±1] crossing. The spectrum is dominated by the pronounced FP resonance around 760 nm. The band gap at the SM[±1] crossing has negative polarity. (b) Contour plot when the top metal surface is immersed in water. The FP resonance is shifted towards 900 nm and the DM[±1] crossing has positive polarity.

shape were attributed to the phenomenological Fano-type interference between resonant SPP reemission and nonresonant transmission through the nanoslit waveguide channel.[17,18] In our experiments also, for the SM[±1] band, the resonance is redshifted and the steep slope of the asymmetric line is on the short-wavelength side of the resonance [Fig. 1(d)].

In addition to those SPP resonances, a broad and only weakly angle-dependent resonance is found around 760 nm. This new resonance, not observed in 2D hole arrays, has been predicted to arise from the resonant enhancement of transmission through the cavity that is formed by the nanoslit waveguide itself.[22–24] Here, incident light is directly coupled into and multiply reflected inside the waveguide channel before being transmitted on the other side of thin film. This FP-type resonance is expected to contribute to the transmission through 1D slits, but not through 2D holes, because only 1D slits support a propagating waveguide mode even in the limit of vanishing slit width. Similar FP resonances have been observed in the microwave region for slit arrays in the limit of $h \gg \lambda_{SP}$.[25] When the sample is immersed in water [Fig. 1(d)], the FP resonance shifts to longer wavelengths (900 nm) and this shift scales approximately linearly with the refractive index $n_d \simeq \epsilon_d^2$ of the immersing liquid [Fig. 1(e)].

In our slit structures, both the shift λ_{SP}-λ_{SP}^0 and the asymmetry of the individual SPP resonances changes sign when the resonance is on the blue side of the FP resonance. This is exemplified in Fig. 1(d) for the DM(1) and SM[1] resonances for $n_d=1.33$ and also observed for all other dielectric media that we investigated.

The shifting cavity resonance has a profound effect on the formation of SPP band gaps. In fact, depending on whether an SM or DM crossing appears at a longer or shorter wavelength than the FP resonance, the very nature of the band crossing changes. In air [Fig. 2(a)], the FP resonance is at a shorter wavelength than the SM[±1] crossing around 980 nm. Here, a transmission maximum is observed on the red side (1014 nm) of the SM[±1] crossing, whereas the transmission shows a pronounced minimum on the blue side. This appearance of dark and bright transmission modes arises from the radiative coupling between the two SPP modes, resulting in superradiant and subradiant damping of the bright and dark modes, respectively.[18,26] We now introduce the notion of a band-gap polarity and define this polarity as *negative* for the SM[±1] mode, where the bright mode lies on the longer-wavelength side of the crossing. When the sample is immersed in water, $n_d=1.33$, the DM[±1] crossing near 730 nm is on the short-wavelength side of the FP resonance (900 nm) and now displays *positive* polarity; i.e., the bright mode is on the short-wavelength side of the crossing.

Clearly, this change in band-gap polarity is connected to the refractive-index-induced shift of the FP resonance. This is further evidenced in Fig. 3, comparing angle-dependent transmission spectra near the SM[±1] crossing when the sample is immersed in (a) air and (b) oil with $n_d=1.516$. In air, the FP resonance is at 760 nm and the band-gap polarity is negative. The bright mode is redshifted. When oil is added, the dark mode region remains almost unaffected, but the bright mode flips to the short-wavelength side of λ_{SP}^0 ($\theta=0°$) so that the band-gap polarity is now positive. The contour plots in Figs. 3(c) and 3(d) reveal an almost mirror-like symmetry of the band structure in the two cases and the symmetry line lies close to $\lambda=\lambda_{SP}^0$. To see how the SM[±1] band gap evolves with n_d, we subjected our sample to two additional dielectric surrounding media with $n_d=1.33$ and $n_d=1.65$. Figure 4 shows transmission spectra at $\theta=0°$ for the four dielectric surroundings, in (a) air ($n_d=1$), (b) water ($n_d=1.33$), index matching oils (c) $n_d=1.512$, and (d) $n_d=1.65$, together with the experimentally determined band-gap energy E_g. The band-gap energy E_g is measured from λ_{SP}^0 to the bright mode when the incident light has the angle $\theta=0°$. This definition of a band gap is consistent with that of the original paper by Ebbesen *et al.*[5] In air and water, where the band gaps have a negative polarity, the energy gaps E_g

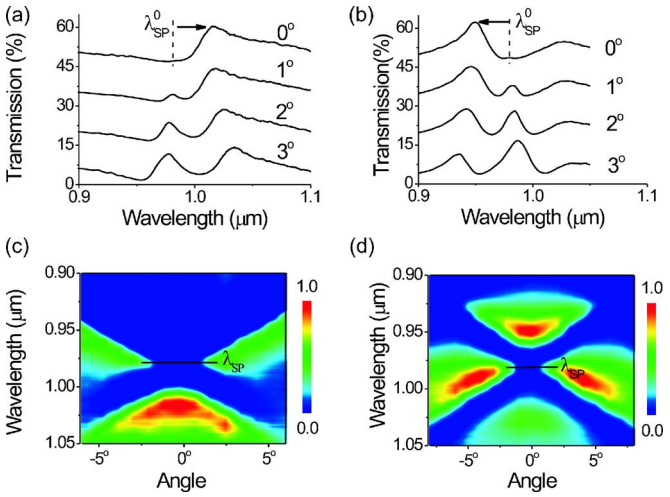

FIG. 3. (Color online) Angle-dependent transmission spectra evidencing polarity flipping of the SM[±1] band gap. (a) Transmission spectra around the SM[±1] crossing for $n_d=1$ (air) and incidence angles between $\theta=0°$ and 3°. (b) Transmission spectra for $n_d=1.512$ (index matching oil). (c) Contour plot around the SM[±1] crossing, showing a negative polarity band gap in air. (d) Same as (c) except that an index matching oil $n_d=1.512$ has been added. The band-gap polarity has changed sign.

are −40 meV and −53 meV, respectively. As the index of refraction changes from 1.33 to 1.512, the band gap flips, now with a positive band gap of 49 meV. Further increasing the index of refraction reduces the band gap to 19 meV, still retaining a positive band gap.

To account for the observed flipping of the band-gap polarity with n_d, we calculated angle-resolved transmission spectra through nanoslit arrays using a dynamical diffraction model.[27,28] This model is particularly appropriate as it allows one to derive analytic expressions for the effect of the FP resonance on both SPP-photon coupling and band-gap formation. The model is based on two major assumptions, both expected to be well fulfilled for the investigated structures. First, a spatially constant surface impedance boundary condition with $Z=\sqrt{1/(\epsilon_d+\epsilon_m)}$ is imposed on the metal/dielectric interfaces, which is known to be a good approximation for highly conductive metals. Second, only a single waveguide mode is considered inside the nanoslit channel. With the incident electric field polarized perpendicular to the slit (y) axis, the magnetic field $H_y(x,z)$ inside the nanoslits is

$$H_y \propto U(x) = I_n^{-1/2}\left[\frac{\eta_d}{\beta}\sin(\beta x)+\cos(\beta x)\right], \qquad (2)$$

with $\eta_d=-ik_0\sqrt{\epsilon_d^2/(\epsilon_d+\epsilon_m)}$, $I_n=\eta_d/\beta^2+\frac{a}{2}[1+(\eta_d/\beta)^2]$, and $k_0=2\pi/\lambda_0$ being the wave vector of the incident wave in vacuum. Here, β is the lowest eigenvalue of the characteristic equation $\tan(\beta a)=2\eta_d\beta/(\beta^2-\eta_d^2)$. In our case, the single-mode approximation is well fulfilled as only the lowest eigenmode, with propagation constant $k_z=\mu=\sqrt{\epsilon_d k_0^2-\beta^2}$ perpendicular to the film, is propagating and weakly damped on a scale of the film thickness h. All higher modes decay within few nanometers only.

Using this diffraction model, angle-dependent transmission spectra are calculated by taking the measured values for the array period and sample thickness. The simulations are performed by fitting the spectral variation of ϵ_m to experimental data and for various refractive indices n_d between 1.0 and 1.7 [Figs. 5(a)–5(d)]. The pronounced transmission enhancement due to the Fabry-Perot resonance and the redshift of the FP resonance with increasing refractive index n_d is

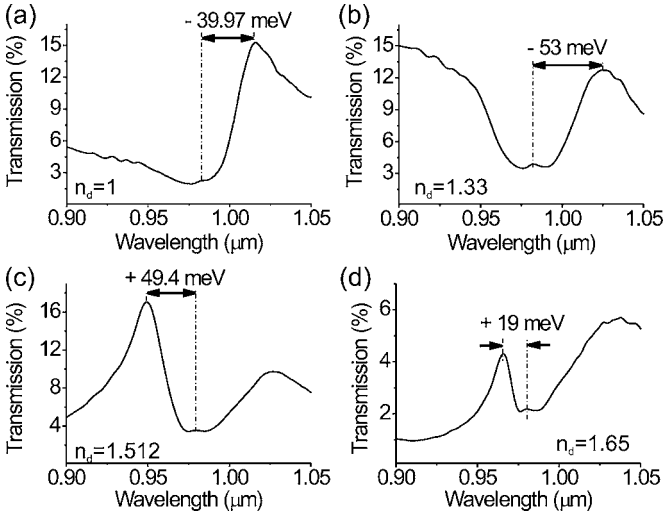

FIG. 4. Measured transmission spectra and plasmonic band gaps of the SM[±1] crossing for a $d=537$ nm immersed in four different dielectric media (a) in air ($n_d=1.0$), (b) in water ($n_d=1.33$), and in two different immersion oils (c) $n_d=1.512$ and (d) $n_d=1.65$.

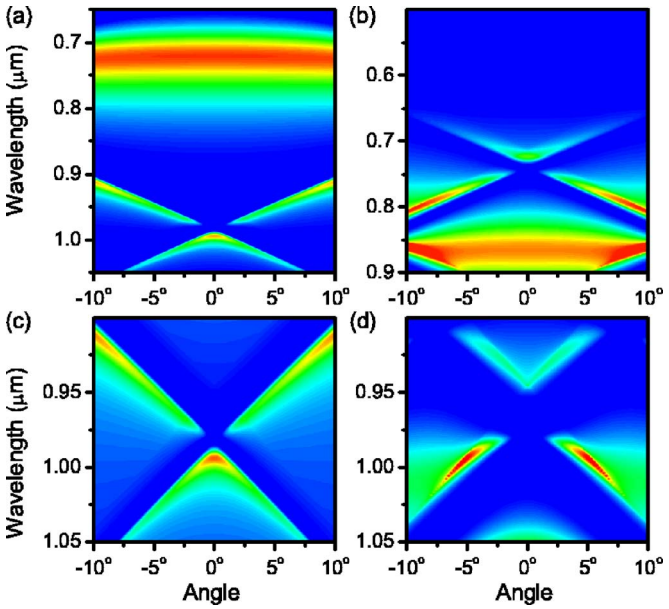

FIG. 5. (Color online) Angle-dependent transmission spectra through nanoslit arrays in a $h=75$ nm thick gold film, calculated using the dynamic diffraction model (Refs. 27 and 28). The calculations are performed for an array period of $d=537$ nm and different refractive indices n_d of the embedding dielectric: (a) $n_d=1.0$, (b) $n_d=1.33$, (c) $n_d=1.0$ (SM[±1] crossing), and (d) $n_d=1.512$. In all cases, a slit width of $a=10$ nm is assumed to approximately match the experimental FP resonances.

evidenced in Figs. 5(a) and 5(b), in good agreement with Figs. 2(a) and 2(b). Figures 5(c) and 5(d) highlight the effect of the shift in FP resonance on the transmission spectra near the SM[±1] crossing. The results clearly demonstrate the negative polarity of the band gap when, for $n_d=1$, the FP resonance is on the high-energy side of the crossing. Increasing n_d to 1.516 shifts the FP resonance to 1120 nm and leads to a change in sign of the band-gap polarity, in agreement with the experimental observation [Figs. 3(c) and 3(d)].

As for the band-gap evolution with n_d, the theoretical band-gap energies E_g are −16 meV, −59 meV, +48 meV, and +32 meV in $n_d=1$, $n_d=1.33$, $n_d=1.516$, and $n_d=1.65$, respectively. These values are slightly different from the experimental results, but the tendency shows a qualitative agreement with Fig. 4, especially the relatively abrupt flipping of the band gap from −53 to +49 meV between $n_d=1.33$ and $n_d=1.516$. When the FP resonance is near the SM[±1] resonace, the coupling between both resonances causes a broadening of the SP transmission line shape and a larger energy band gap E_g at the SM[±1] resonance.

The diffraction model provides clear insight into the physics underlying the band-gap polarity flipping. First, an approximate analytic expression can be derived for the radiative coupling V between the individual SPP resonances and the zeroth-order transmission mode, propagating into the far field:

$$\frac{V}{\hbar c} = -\mu \cot(\mu h)\left[\int_0^a U(x)dx\right] \Big/ d \simeq -(a/d)\mu \cot(\mu h). \tag{3}$$

The imaginary part of V directly gives the SPP radiative lifetime $T_{1,r}=1/[2\hbar\ \mathrm{Im}(V)]$, whereas the real part of V contributes to the shift between the SPP resonance on the nanostructured metal film and λ_{SP}^0. For a narrow slit with $a/d \ll 1$, we find a shift $\delta\lambda=\lambda_{SP}-\lambda_{SP}^0$ of

$$\frac{\delta\lambda[p]}{\lambda_{SP}^0[p]} = \left[\frac{a}{d}\frac{\epsilon_d}{\epsilon_m} - \frac{iV}{\hbar c}\sqrt{\frac{\epsilon_d}{\epsilon_m}}\frac{d}{2\pi p}\right] + O(a^2/d^2). \tag{4}$$

Equation (3) essentially shows that the coupling between evanescent SPP modes and the propagating zeroth-order far-field mode is mediated via the nanoslit waveguide cavity. This radiative coupling is greatly enhanced when the SPP and cavity mode are in resonance—i.e., for $\mathrm{Re}(\mu)h \simeq n\pi$, $n=1,2,\ldots$. Rewriting μ in terms of an effective refractive index n_e, $\mu=n_e k_0$, gives the nanoslit FP resonances $\lambda_{FP}=2\mathrm{Re}(n_e)h/n$. Tuning the SPP wavelength across λ_{FP} leads to a change in sign of V and, thus, to a π phase change of the reemitted SPP wave. This phase change is the origin of the transition from a redshifted Fano-type transmission profile $[\mathrm{Re}(\delta\lambda)>0]$ for $\lambda_{SP}>\lambda_{FP}$ to a blueshifted asymmetric line for $\lambda_{SP}<\lambda_{FP}$ [Fig. 1(c)]. In addition to this radiative damping, the local variation in refractive index due to the nanoslits leads to a small shift $a\epsilon_d/d\epsilon_m$ of the SPP resonance, as expected from an effective medium model.

A similar expression as for the radiative coupling can be derived for the nanoslit-induced coupling $W_{p,q}$ between two different SPP resonances p and q at the same interface. With $\alpha_p=k_0 \sin\theta+pG$ and coupling integrals $J_p=\frac{1}{d}\int_0^a e^{-i\alpha_p x}U(x)dx$ and $K_p=\int_0^a e^{i\alpha_p x}U(x)dx$, one finds

$$W_{p,q} = \hbar c \mu \epsilon_d [\sin(\mu h)]^{-1} J_p K_q. \tag{5}$$

The real part of the coupling, $\mathrm{Re}(W)$, corresponds to the energy of the band gap which opens up at the crossing of the two resonances. The imaginary part $\mathrm{Im}(W)$ accounts for the radiative coupling of the two resonances, which gives rise to the strong difference in radiative damping of the dark and bright modes.[18] Equation (5) indicates that both the band-gap energy and the radiative coupling are resonantly enhanced when the crossing is close to the FP resonance. This demonstrates that SPP coupling to nanoscale waveguide cavities is an efficient, novel, and general concept for tailoring SPP band gaps. Tuning the SPP crossing from the high- to low-energy side of the FP resonance, as experimentally achieved by varying the refractive index of the embedding dielectric, changes the sign of $\mathrm{Re}(W)$ and, thus, accounts for the observed flipping of the band-gap polarity.

While the diffraction model accounts nicely for the experimental findings, in particular the band-gap flipping, we did not yet achieve a full quantitative match. To account for the values of λ_{FP}, a small slit width of only 10 nm has to be assumed. In air, we observe the fundamental Fabry-Perot resonance at 760 nm. With $\lambda_{FP}=2\mathrm{Re}(n_e)h$, this corresponds to an effective refractive index of the waveguide mode of $n_e \simeq 5$. In the simulations, such a high value of n_e is only reached for extremely narrow waveguides. We have tried to resolve this discrepancy by assuming a less idealized, slightly nonrectangular shape of the waveguide in the model simulation but essentially failed to reach a more quantitative agreement. Also, in other samples, we find such a quantitative discrepancy between experiment and simulation. In the much thicker ($h=150$ nm) samples studied in Ref. 18, e.g., we observe no FP resonance in the investigated wavelength range (650–950 nm), but find it only much further in the infrared. At this point, we believe that this discrepancy between experiment and theory is evidence of an incomplete understanding of the effective refractive index of such nanoscale waveguides. Experimentally measuring the refractive index of such nanoscale waveguides independently therefore is highly desirable, yet beyond the scope of this paper.

The diffraction calculations indicate that the flipping of the band-gap polarity is intimately connected with a change in the spatial structure of the SPP eigenmodes of the plasmonic crystal. Analytical calculations show that the ratio E_{slit}/E_{pl} between the local electric field E_{slit} inside the nanoslit at the metal/dielectric interface and the field at a nearby planar interface E_{pl} is the characteristic quantity defining the band-gap polarity. A local enhancement of the electric field $E_{slit}/E_{pl}>1$ results in redshifted SPP modes and negative polarity band gaps typical of 2D hole arrays. In nanoslit arrays, however, the interference of the incident field with the field propagating inside the nanoslit waveguide may result in $E_{slit}/E_{pl}<1$—often even in negative values of E_{slit}—giving rise to blueshifted SPP resonances and a change in the band-gap polarity. The pronounced sensitivity of the slit field to the local dielectric function makes it interesting

to explore SPP field imaging in nanoscopic sensing applications.

In conclusion, we have studied the effect of a nanoscale waveguide cavity on the band-gap formation in quasi-one-dimensional plasmonic nanocrystals. Coherent coupling of surface plasmon polaritons to a nanoslit cavity gives rise to a pronounced resonant enhancement of the band-gap energy, leading even to an effective flipping of the band-gap polarity. In the investigated structures, the band-gap enhancement is intimately connected with an increase in radiative damping. One can envision that both quantities can be decoupled in multiply stacked layers of plasmonic nanostructures. Our results indicate that this is an important future direction in surface-plasmon-polariton band-gap engineering.

Financial support of the work in Korea by MOST, MOCIE, and KOSEF and that in Germany by the DFG (Grant No. SFB296) is gratefully acknowledged.

*Electronic address: denny@snu.ac.kr

[1] K. v. Klitzing, G. Dorda, and M. Pepper, Phys. Rev. Lett. **45**, 494 (1980).
[2] D. Bimberg, M. Grundmann, and N. N. Ledentsov, *Quantum Dot Heterostructures* (Wiley, Chichester, UK, 1999).
[3] J. D. Joannopoulos, R. D. Meade, and J. N. Winn, *Photonic Crystals: Molding the Flow of Light* (Princeton University Press, Princeton, 1995).
[4] E. Yablonovitch, Phys. Rev. Lett. **58**, 2059 (1987).
[5] T. W. Ebbesen, H. J. Lezec, H. F. Ghaemi, T. Thio, and P. A. Wolff, Nature (London) **391**, 667 (1998).
[6] E. Altewischer, M. P. van Exter, and J. P. Woerdman, Nature (London) **418**, 304 (2002).
[7] H. J. Lezec, A. Degiron, E. Devaux, R. A. Linke, L. Martín-Moreno, F. J. García-Vidal, and T. W. Ebbesen, Science **297**, 820 (2002).
[8] S. C. Hohng, Y. C. Yoon, D. S. Kim, V. Malyarchuk, R. Müller, Ch. Lienau, J. W. Park, K. H. Yoo, J. Kim, H. Y. Ryu, and Q. H. Park, Appl. Phys. Lett. **81**, 3239 (2002).
[9] S. Linden, C. Enkrich, M. Wegener, J. Zhou, T. Koschny, and C. M. Soukoulis, Science **306**, 1351 (2004).
[10] I. I. Smolyaninov, C. C. Davis, V. N. Smolyaninova, D. Schaefer, J. Elliott, and Anatoly V. Zayats, Phys. Rev. B **71**, 035425 (2005).
[11] P. A. Andrew and W. L. Barnes, Science **306**, 1002 (2004).
[12] D. J. Bergman and M. I. Stockman, Phys. Rev. Lett. **90**, 027402 (2003).
[13] See, e.g., W. L. Barnes, T. W. Preist, S. C. Kitson, and J. R. Sambles, Phys. Rev. B **54**, 6227 (1996).
[14] D. S. Kim, S. C. Hohng, V. Malyarchuk, Y. C. Yoon, Y. H. Ahn, K. J. Yee, J. W. Park, J. Kim, Q. H. Park, and Ch. Lienau, Phys. Rev. Lett. **91**, 143901 (2003).
[15] H. F. Ghaemi, T. Thio, D. E. Grupp, T. W. Ebbesen, and H. J. Lezec, Phys. Rev. B **58**, 6779 (1998).
[16] C. Genet, M. P. van Exter, and J. P. Woerdman, Opt. Commun. **225**, 331 (2003).
[17] M. Sarrazin, J. P. Vigneron, and J. M. Vigoureux, Phys. Rev. B **67**, 085415 (2003).
[18] C. Ropers, D. J. Park, G. Stibenz, G. Steinmeyer, J. Kim, D. S. Kim, and C. Lienau, Phys. Rev. Lett. **94**, 113901 (2005).
[19] C. Ropers, G. Stibenz, G. Steinmeyer, R. Müller, D. J. Park, K. G. Lee, J. E. Kihm, J. Kim, Q. H. Park, D. S. Kim, and C. Lienau, Appl. Phys. B: Lasers Opt. **84**, 183 (2006).
[20] L. Martín-Moreno, F. J. García-Vidal, H. J. Lezec, K. M. Pellerin, T. Thio, J. B. Pendry, and T. W. Ebbesen, Phys. Rev. Lett. **86**, 1114 (2001).
[21] E. Popov, M. Neviere, S. Enoch, and R. Reinisch, Phys. Rev. B **62**, 16100 (2000).
[22] J. A. Porto, F. J. García-Vidal, and J. B. Pendry, Phys. Rev. Lett. **83**, 2845 (1999).
[23] F. J. García-Vidal and L. Martín-Moreno, Phys. Rev. B **66**, 155412 (2002).
[24] Y. Takakura, Phys. Rev. Lett. **86**, 5601 (2001).
[25] H. E. Went, A. P. Hibbins, J. R. Sambles, C. R. Lawrence, and A. P. Crick, Appl. Phys. Lett. **77**, 2789 (2000).
[26] R. H. Dicke, Phys. Rev. **93**, 99 (1954).
[27] H. Lochbihler, Phys. Rev. B **50**, 4795 (1994).
[28] K. G. Lee and Q. Han Park, Phys. Rev. Lett. **95**, 103902 (2005).